03,10

Investigation of nanocrystalline and traditionally produced thermoelectric materials on the basis of $Bi_2Te_{3-x}Se_x$, $Bi_{2-x}Sb_xTe_3$, PbTe and GeTe

© Yu.I. Shtern[1], A.A. Sherchenkov [1], M.Yu. Shtern[1], M.S. Rogachev[1,¶], N.Yu. Tabachkova[2]

[1] National Research University of Electronic Technology, Zelenograd, Moscow, Russia
[2] National University of Science and Technology MISiS, Moscow, Russia

¶E-mail: m.s.rogachev88@gmail.com

Received October 29, 2024
Revised October 14, 2025
Accepted October 24, 2025

Efficient thermoelectric materials on the basis of $Bi_2Te_{3-x}Se_x$, $Bi_{2-x}Sb_xTe_3$, PbTe and GeTe for temperature range of 200−900 K were investigated. Materials were fabricated using traditional methods and nanostructuring. A comparative analysis of the main physical parameters of these materials was carried out, and the temperature dependences of their thermoelectric parameters and thermoelectric figure of merit were determined. The relationship between structure and thermoelectric parameters in nanocrystalline materials was established. A study of heat transport mechanisms showed that a 10−21 % increase in thermoelectric figure of merit in nanocrystalline materials is due to a decrease in phonon thermal conductivity. As a result of the calculation of a three-section thermoelement, in which nanocrystalline thermoelectric materials were used, a high efficiency of 18 % was obtained at temperatures of 300−900 K.

Keywords: thermoelectric materials, nanostructure, thermoelectric parameters, heat transport mechanisms.

DOI: 10.61011/PSS.2025.10.62627.286-25

1. Introduction

Thermoelectricity has been one of the most actively developing areas in science and technology in recent years. The benefits, as well as the huge untapped potential of using thermoelectricity to regulate temperature (Peltier effect) and generate electrical energy (Seebeck effect), attract high interest in it. The non-alternative areas of application of thermoelectricity are worth-mentioning: precision temperature control, power supply to spacecraft during deep space exploration, as well as hard-to-reach territories.

The efficiency of thermoelectric energy conversion is largely determined by the thermoelectric figure of merit ($Z = s^2\sigma/\kappa$, where s — Seebeck coefficient, σ — electrical conductivity, κ — thermal conductivity) of semiconductor materials used for the manufacture of thermoelements — fundamentals of the design of any thermoelectric device. Therefore, one of the main tasks of thermoelectric materials science is to optimize the thermoelectric parameters (s, σ, κ) of thermoelectric materials. The following ways of increasing Z are obvious: increasing the power factor ($s^2\sigma$) and reducing the thermal conductivity of thermoelectric materials.

The development of effective thermoelectric materials is carried out in two directions. One is related to the search for new compositions of thermoelectric materials [1–5], and the other is related to the use of nanotechnology to produce nanostructured thermoelectric materials. In the second case, technology is used to create nanocrystalline materials [6–12], or composites with nanoscale inclusions of foreign phases or compounds [7–9] are obtained.

A number of scientific groups is involved in development of effective thermoelectric materials [9,13–15]. However, despite the enormous progress in thermoelectric materials science due to the developments of new thermoelectric materials, chalcogenides based on Bi_2Te_3, PbTe and GeTe are today the main semiconductor materials used for the manufacture of thermoelectric energy converters. The compounds and methods of producing such thermoelectric materials have been developed, which generally include, zone melting (ZM), extrusion (Ex), hot pressing (HP), super-fast cooling of melts, Bridgman method, spark plasma sintering (SPS).

Analyzing the latest achievements in creating effective thermoelectric materials, we can draw the following conclusion. In a number of studies, a rise in Z has been achieved by increasing the power factor [8,12,13]. At the same time, there are significantly more publications stating that higher efficiency may be achieved by reducing thermal conductivity [7–9,16]. The mechanisms of heat transport are considered in [8,17–19], and the sizes of crystallites necessary to reduce the contribution of phonons are — in [20–23], where the use of nanomaterials is justified.

However, despite the impressive successes achieved by nanostructuring of thermoelectric materials, they are far from practical implementation in thermoelectric devices. At the moment, there is no deep understanding of the mechanisms of thermal conductivity, carrier transport and scattering in these complex materials, as well as the stability of their properties. For this purpose, it is advisable to fabricate and make comparative studies of thermoelectric

Table 1. Compounds, methods and ranges of operating temperatures for thermoelectric materials

Temperature range	Components of thermoelectric materials	Type of conductivity	Method
Low-temperature 200–400 K	$Bi_2Te_{2.8}Se_{0.2}$ (0.16 wt.% $CdCl_2$)	*n*	ZM, SPS
	$Bi_{0.5}Sb_{1.5}Te_3$ (2.20 wt.% Te and 0.16 wt.% TeI_4)	*p*	ZM, SPS
Medium-temperature 400–600 K	$Bi_2Te_{2.4}Se_{0.6}$ (0.16 wt.% CuBr)	*n*	Ex, SPS
	$Bi_{0.4}Sb_{1.6}Te_3$ (0.14 wt.% $PbCl_2$ and 1.80 wt.% Te)	*p*	Ex, SPS
Medium-temperature 600–900 K	PbTe (0.30 wt.% PbI_2 and 0.30 wt.% Ni)	*n*	HP, SPS
	GeTe (7.20 wt.% Bi)	*p*	HP, SPS

materials obtained by traditional methods (classical materials) and nanocrystalline materials of the same composition.

In connection with the above, the purpose of this work is to obtain effective thermoelectric materials using traditional methods and nanostructuring for the operating temperature range 200–900 K, to conduct research and comparative analysis of the main physical parameters, as well as to determine the influence of heat transport mechanisms on thermoelectric figure of merit.

2. Experimental

Thermoelectric materials based on chalcogenides were fabricated using traditional methods of zone melting, extrusion and hot pressing for the operating temperature range from 200 to 900 K (Table 1). In order to increase the thermoelectric figure of merit, conditions to fabricate nanocrystalline thermoelectric materials by spark plasma sintering have been developed, including the manufacture of nano-dispersed powders and their compaction to create bulk samples of thermoelectric materials [24]. Thermoelectric materials were synthesized by direct fusion of components in sealed quartz tubes placed in a muffle rocking furnace under the following conditions: for materials based on Bi_2Te_3 and Sb_2Te_3 — 1050 K, 120 min; for material based on PbTe — 1350 K, 120 min; for material based on GeTe — 1250 K, 180 min. After synthesis the tubes with thermoelectric materials were quenched with a cooling rate of about 500 K/min. Synthesized materials were crushed using a CSchD-6 crusher and a knife-type mill IKA A11 to a particle size of 250 μm. Further, some of the powders were used to produce bulk materials using traditional methods: zone melting, extrusion or hot pressing. Another part of the powders intended for the production of nanocrystalline materials using SPS was additionally crushed in a high-energy planetary ball mill „Retsch PM400 MA“. The same ingots of materials synthesized by direct fusion were used for the fabrication of nanocrystalline materials and materials obtained by traditional methods. The composition of the materials and alloying components are presented in Table 1.

Thermoelectric materials $Bi_2Te_{2.8}Se_{0.2}$ and $Bi_{0.5}Sb_{1.5}Te_3$ were obtained by zone melting at a temperature in the molten zone of 950 K, the movement speed of the zone is 0.4 mm/min, the number of passes of the zone is two. After zone melting, before depressurization of the test tubes, the thermoelectric materials were subjected to homogenizing annealing at a temperature of 650 K for 20 h. $Bi_2Te_{2.4}Se_{0.6}$ was extruded at 4.0 t per 1 cm^2, and $Bi_{0.4}Sb_{1.6}Te_3$ at a pressure of 3.5 t per 1 cm^2, at temperatures of 680–700 K and 690–710 K, respectively. The fabricated ingots were subjected to the stabilizing annealing in Ar atmosphere at 680 K for ingots $Bi_2Te_{2.4}Se_{0.6}$ and 650 K for ingots $Bi_{0.4}Sb_{1.6}Te_3$ for 48 and 24 h, respectively. Hot pressing of PbTe and GeTe was carried out at a pressure of 450 MPa and a temperature of 690 K for 5 min, followed by annealing at 770 K in argon atmosphere for 48 h.

Bulk samples of nanocrystalline thermoelectric materials were obtained as follows. DC current (up to 1200 A) was passed through the powder loaded into the graphite mold of SPS 511S system in a pulsed mode with a pulse duration of up to 12 ms and intervals of 2 ms. At the same time, controlled pressure was applied to the powder. The process temperature was adjusted automatically due to the value of the passed current. Samples of nanocrystalline thermoelectric materials with a diameter of 20 mm and a height of 3 to 10 mm were obtained from SPS powders crushed in a planetary ball mill at a speed of 400 rpm for 60 min. Optimal parameters for SPS were determined: for materials on the basis of $Bi_2Te_{2.8}Se_{0.2}$, $Bi_{0.5}Sb_{1.5}Te_3$, $Bi_2Te_{2.4}Se_{0.6}$, $Bi_{0.4}Sb_{1.6}Te_3$, PbTe — 723 K, 5 min; GeTe — 773 K, 5 min. During SPS process the pressure was 50 MPa for materials on the basis of $Bi_2Te_{2.8}Se_{0.2}$; $Bi_{0.5}Sb_{1.5}Te_3$; $Bi_2Te_{2.4}Se_{0.6}$; $Bi_{0.4}Sb_{1.6}Te_3$; GeTe and 80 MPa for material on the basis of PbTe. SPS of nano-dispersed powders of thermoelectric materials was carried out in an inert gas environment.

The size, phase composition, and fine structure of nano-dispersed powders and nanocrystalline thermoelectric materials were studied by transmission electron microscopy (TEM) using JEM-2100 system at an accelerating voltage of 200 kV. The powder compositions were determined according to the parameters of the crystal lattice. The size of crystallites was determined by the broadening of the peaks on X-ray diffraction pattern with an accuracy of ± 2 nm.

The density of nanocrystalline materials was measured by hydrostatic weighing with an error of no more than 0.01 g/cm^3. Three density measurements (ρ) were performed for each sample and the average value was calculated.

To determine the concentration and mobility of charge carriers, the results of measuring the Hall constant on HMS-5000 (Ecopia) system at 300 K in a magnetic field of 0.55 T, at a current of 10 mA were used. Samples with sizes $7 \times 7 \times 4\,\text{mm}^3$ were prepared for the studies. The concentration of the majority charge carriers (n) and their mobility (μ) were determined as follows:

$$n = 1/e\,R_{\text{H}}; \quad \mu = \sigma\,R_{\text{H}}, \tag{1}$$

where R_{H} — Hall constant, e — charge of the electron.

Microhardness was measured using Vickers method with PMT-3M microhardness tester based on the recovered indenter print.

To control possible phase transformations during heat treatment, accompanied by thermal effects, studies were conducted using differential scanning calorimetry methods (Shimadzu DSC-50 calorimeter).

Studies of the temperature dependences of the thermoelectric parameters of classical and nanocrystalline thermoelectric materials in the range from 200 to 900 K were carried out using method presented in [25]. The studies were conducted in a stationary mode in a single measuring cycle, the thermal conductivity was determined by the absolute method. Thermoelectric parameters of materials based on Bi_2Te_3 and Sb_2Te_3 were measured: perpendicular to SPS pressure orientation; parallel to the direction of pressure during extrusion; parallel to the direction of crystallization during zone melting. The measurement directions of the thermoelectric parameters coincided with the direction of the current in the legs of the thermoelectric element.

Thermal conductivity was calculated by the formula:

$$\kappa = LQ/(S\Delta T), \tag{2}$$

where Q — heat flow passing through the sample; ΔT — temperature difference on the sample; L — height of the sample; S — area of the sample cross-section. The heat flow was calculated based on the power of the gradient heater minus the heat losses along the supply potential wires. In order to reduce the measurement error of thermal conductivity, the installation was calibrated using reference samples: quartz glass KV (GOST 15130-86) and alloy VT6 (GOST 19807-91).

Thermal conductivity was calculated by the formula:

$$\sigma = \frac{2LI}{S(U_1 + U_2)}, \tag{3}$$

where I — dc current passing through the sample; U_1 and U_2 — voltage drop across the sample in opposite current directions.

The Seebeck coefficient of the investigated material is determined as follows. Thermal EMF was measured on a sample using the same legs of thermocouples E_{c-c} and E_{a-a}

$$s_1 = E_{c-c}/\Delta T, \tag{4}$$

$$s_2 = E_{a-a}/\Delta T. \tag{5}$$

From the data obtained (s_1 and s_2), the Seebeck coefficients values of alumel and chromel were excluded, and the average value of Seebeck coefficient of the thermoelectric material was calculated.

The error of the method is 2% for the coefficients of Seebeck and electrical conductivity, 5% for the coefficient of thermal conductivity.

3. Results and discussion

It has been established that when nano-dispersed powders are produced in a planetary ball mill, intensive grinding of thermoelectric materials occurs in the first 20–40 min, and the minimum powder sizes are reached after 50–60 min. For all thermoelectric materials, except PbTe, the minimum sizes of powder crystallites were reached at the level of 24–29 nm. For PbTe these sizes were much greater and were about 84 nm. The average crystallite sizes of powders of thermoelectric materials obtained during 60 min grinding are shown in Table 2. Here and further, the compositions of thermoelectric materials are indicated without alloying.

As an example, Figure 1 shows TEM-images of agglomerates and individual powder particles after grinding for 60 min. All powders were found to be single-phase, and the powder compositions corresponded to those of synthesized thermoelectric materials. Micro-deformations of the crystal structure were found in these powders, which change slightly at different grinding times.

Studies of the fine structure and phase composition of nanocrystalline thermoelectric materials were carried out using transmission electron microscopy with examination of electron diffraction patterns. As an example, Figure 2 illustrates TEM-images of structures of thermoelectric materials based on $Bi_2Te_{2.8}Se_{0.2}$ and $Bi_{0.5}Sb_{1.5}Te_3$.

The lattice parameters of bulk nanocrystalline thermoelectric materials were determined. It was found that the fabricated materials and synthesized materials had equivalent compositions. The distribution of elements in the thermoelectric materials was homogeneous. The

Table 2. Average crystallite sizes in powders and thermoelectric materials

Thermoelectric material	Average crystallite sizes, nm	
	Powders	Bulk thermoelectric materials, obtained by SPS
$Bi_2Te_{2.8}Se_{0.2}$	28	97
$Bi_{0.5}Sb_{1.5}Te_3$	29	76
$Bi_2Te_{2.4}Se_{0.6}$	28	74
$Bi_{0.4}Sb_{1.6}Te_3$	28	78
PbTe	84	116
GeTe	24	72

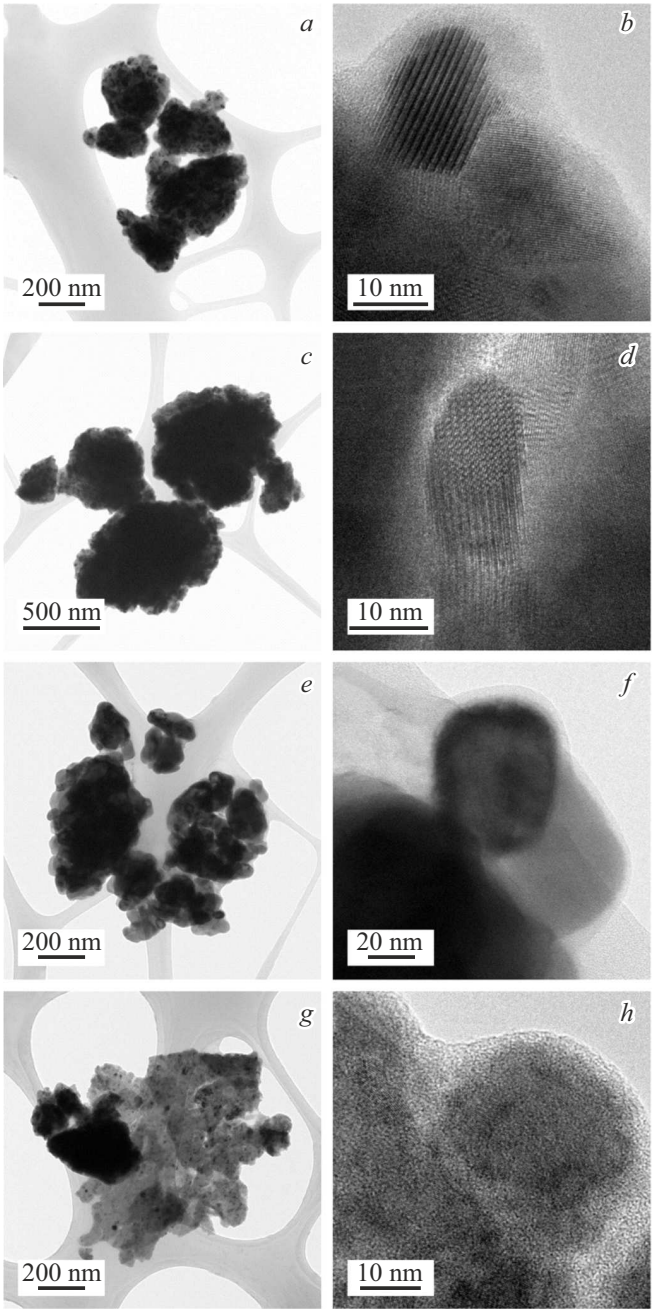

Figure 1. TEM images of agglomerates (*a*) $Bi_2Te_{2.8}Se_{0.2}$, (*c*) $Bi_{0.5}Sb_{1.5}Te_3$, (*e*) PbTe, (*g*) GeTe and individual powder particles (*b*) $Bi_2Te_{2.8}Se_{0.2}$, (*d*) $Bi_{0.5}Sb_{1.5}Te_3$, (*f*) PbTe, (*h*) GeTe.

distribution of reflexes on the ring electron diffraction patterns shown in Figure 2 correspond to solid solutions of $Bi_2Te_{2.8}Se_{0.2}$ and $Bi_{0.5}Sb_{1.5}Te_3$. The size of crystallites were identified in thermoelectric materials. A comparison of the data obtained shows that the size of crystallites after sintering for all thermoelectric materials increased compared to the size of the powders. The average sizes of crystallites in bulk nanocrystalline materials obtained from powders ground for 60 min are presented in Table 2.

The main physical parameters have been studied and the data for nanocrystalline and materials obtained by traditional methods, presented in Table 3, have been compared.

According to the data presented, the density of nanocrystalline materials is 97–98 % of the density of materials obtained by direct fusion of components (theoretical density).

The obtained concentration and mobility values for nanocrystalline and classical materials of the same composition have similar values. However, the carrier mobility of nanocrystalline materials is somewhat lower, which is due to their scattering on nanoscale structural elements and impacts the values of electrical conductivity. The microhardness of nanocrystalline materials is higher than that of classical materials [26,27]. This result is consistent with Hall–Petch law stating that nanostructuring increases the mechanical strength of materials [28].

Studies of the thermoelectric parameters of classical and nanocrystalline materials were carried out in the range of their operating temperatures. Figure 3 shows the results of the study of electrical conductivity temperature depen-

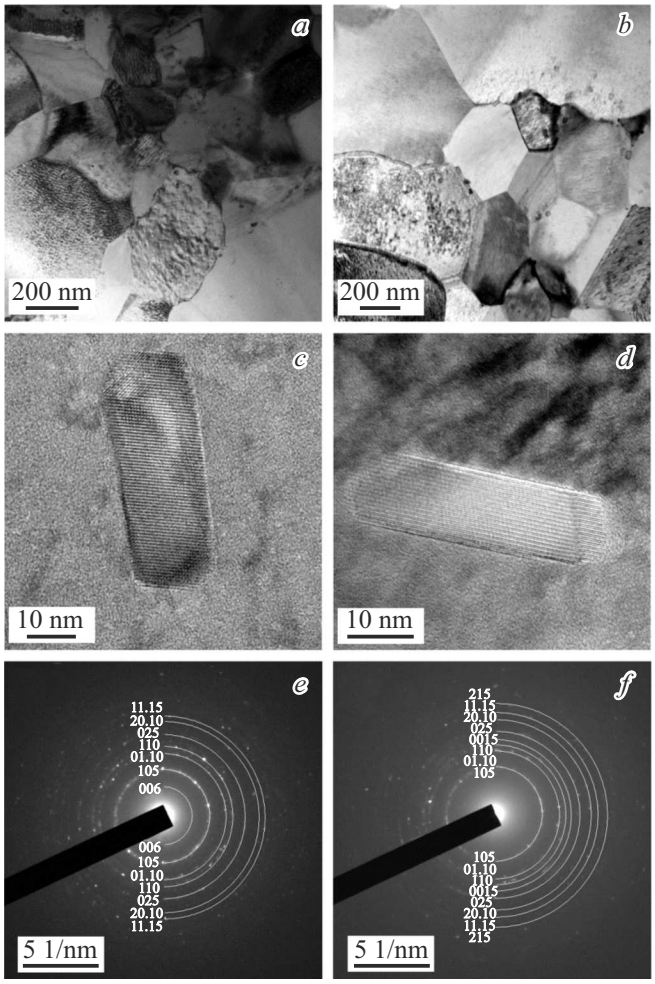

Figure 2. TEM high-resolution images of structures (*a*) $Bi_2Te_{2.8}Se_{0.2}$ and (*b*) $Bi_{0.5}Sb_{1.5}Te_3$, of individual crystallites (*c*) $Bi_2Te_{2.8}Se_{0.2}$ and (*d*) $Bi_{0.5}Sb_{1.5}Te_3$, electron diffraction patterns (*e*) $Bi_2Te_{2.8}Se_{0.2}$ and (*f*) $Bi_{0.5}Sb_{1.5}Te_3$.

Table 3. Properties of thermoelectric materials obtained by various methods

Material	SPS				Synthesis	Traditional methods			
	ρ, g/cm^3	n, 10^{19} cm^{-3}	μ, cm^2/V·s	HV	ρ, g/cm^3	ρ, g/cm^3	n, 10^{19} cm^{-3}	μ, cm^2/V·s	HV
$Bi_2Te_{2.8}Se_{0.2}$	7.60	3.12	232	34.6	7.75	7.74	2.99	242	33.5
$Bi_{0.5}Sb_{1.5}Te_3$	6.65	3.37	203	45.3	6.78	6.78	3.28	217	44.4
$Bi_2Te_{2.4}Se_{0.6}$	7.62	3.47	208	50.2	7.78	7.77	3.37	219	49.9
$Bi_{0.4}Sb_{1.6}Te_3$	6.63	3.80	176	60.9	6.77	6.76	3.67	185	60.1
PbTe	8.11	4.10	188	52.4	8.28	8.03	4.07	201	51.7
GeTe	6.08	10.05	76	127.8	6.20	6.01	9.76	80	125.7

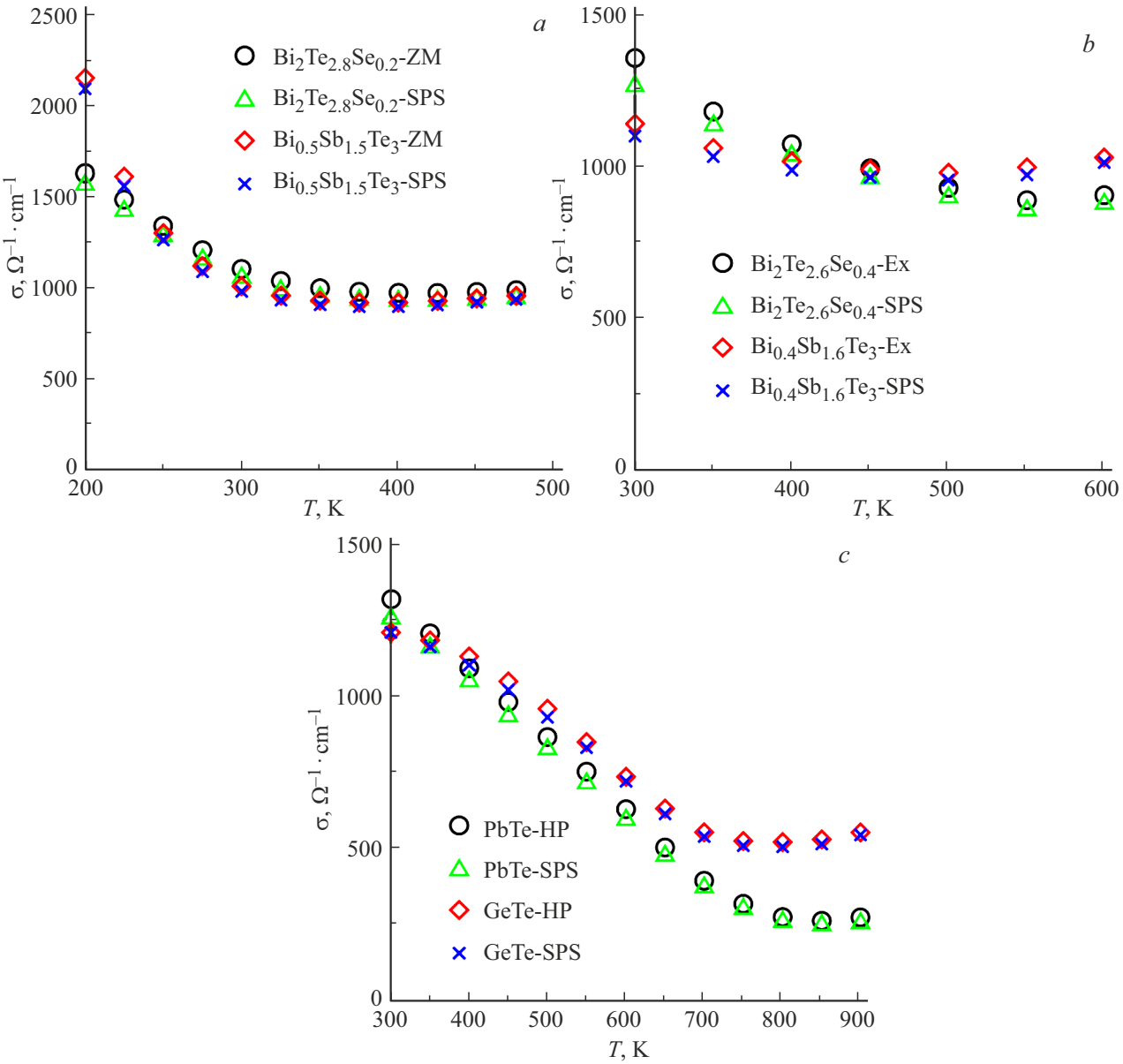

Figure 3. Temperature dependences of electrical conductivity (*a*) $Bi_2Te_{2.8}Se_{0.2}$ and $Bi_{0.5}Sb_{1.5}Te_3$, (*b*) $Bi_2Te_{2.4}Se_{0.6}$ and $Bi_{0.4}Sb_{1.6}Te_3$, (*c*) PbTe and GeTe.

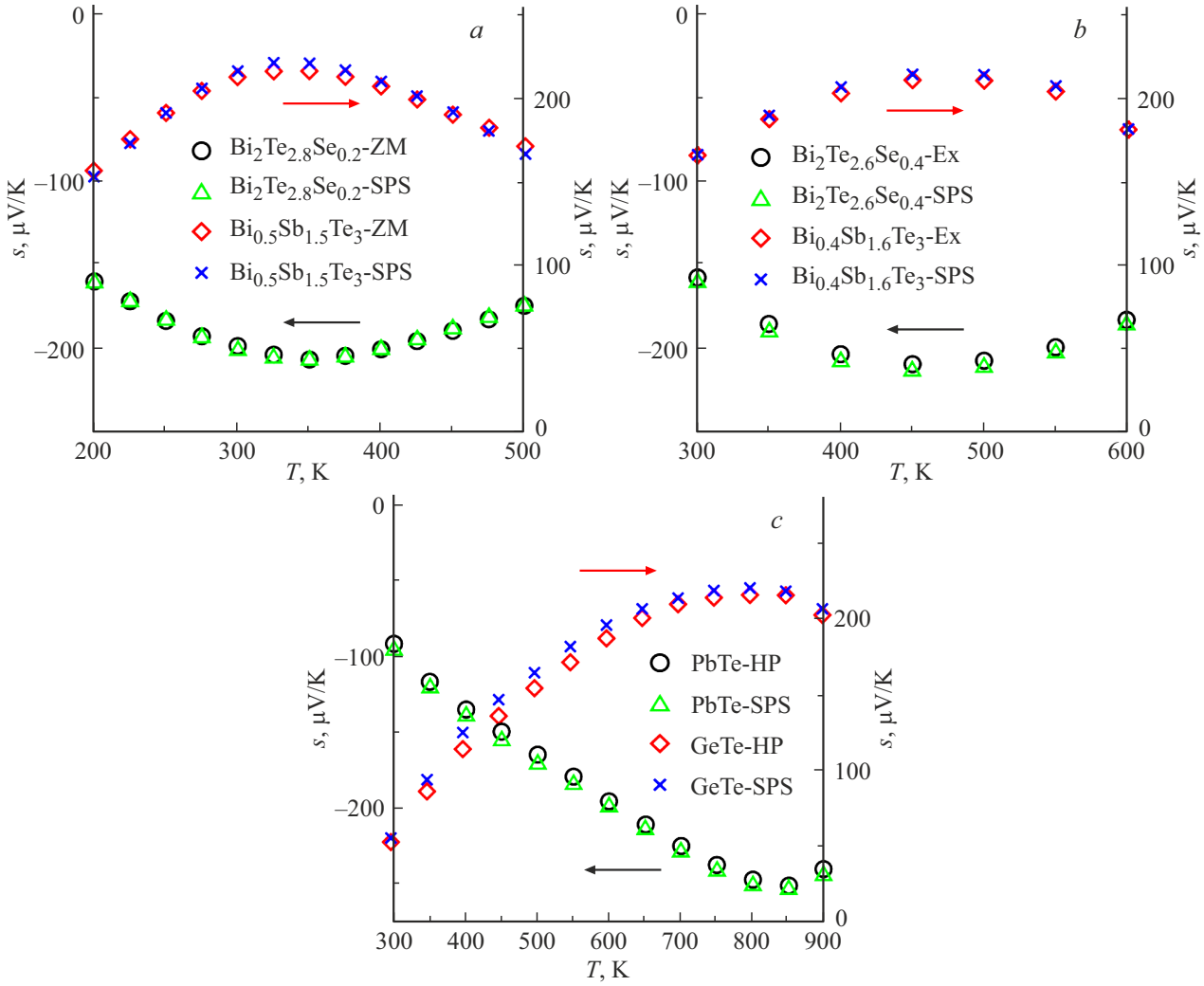

Figure 4. Temperature dependences of Seebeck coefficient (*a*) $Bi_2Te_{2.8}Se_{0.2}$ and $Bi_{0.5}Sb_{1.5}Te_3$, (*b*) $Bi_2Te_{2.4}Se_{0.6}$ and $Bi_{0.4}Sb_{1.6}Te_3$, (*c*) PbTe and GeTe.

dencies for the developed thermoelectric materials. The general nature of the temperature dependences of electrical conductivity indicates that all thermoelectric materials are partially degenerate semiconductor materials in the range of operating temperatures. The electrical conductivity of nanocrystalline materials in the entire temperature range is lower than that of samples obtained by traditional methods by an amount not exceeding 4%. This is explained by the fact that nanocrystalline thermoelectric materials have a slightly lower mobility of charge carriers due to their scattering on nanoscale structural elements.

The Seebeck coefficient for all the studied thermoelectric materials rises with increasing temperature (Figure 4), reaching a maximum for various materials from 200 to 250 μV/K in the temperature range at which the maximum values of their thermoelectric figure of merit are observed. After that, there is a decrease in Seebeck coefficient for all materials, which is associated with an increase in the contribution of minority charge carriers to the electrical transport process. The difference in the Seebeck coefficient of classical and nanocrystalline materials does not exceed the measurement error.

Figure 5 shows experimental data on thermal conductivity (κ_{tot}).

Comparing the experimental values of thermal conductivity of classical and nanocrystalline thermoelectric materials, the following should be emphasized. The values κ_{tot} for all nanocrystalline materials are lower by 12–22%. A decrease in thermal conductivity to 20% was observed in medium-temperature nanocrystalline materials based on $Bi_{2-x}Sb_xTe_3$ and $Bi_2Te_{3-x}Se_x$. Minimal decrease of thermal conductivity of the low-temperature nanocrystalline materials on the basis of $Bi_2Te_{3-x}Se_x$ doesn't exceed 12%, and PbTe — 16%. The thermal conductivity of nanocrystalline material based on GeTe is 22% lower than for the hot-pressed analog.

As noted earlier, the concept of creating nanocrystalline thermoelectric materials is based on reducing the phonon component of thermal conductivity [6,29]. To confirm this fact and determine the mechanisms of heat transport, the calculation was carried out and the contribution of

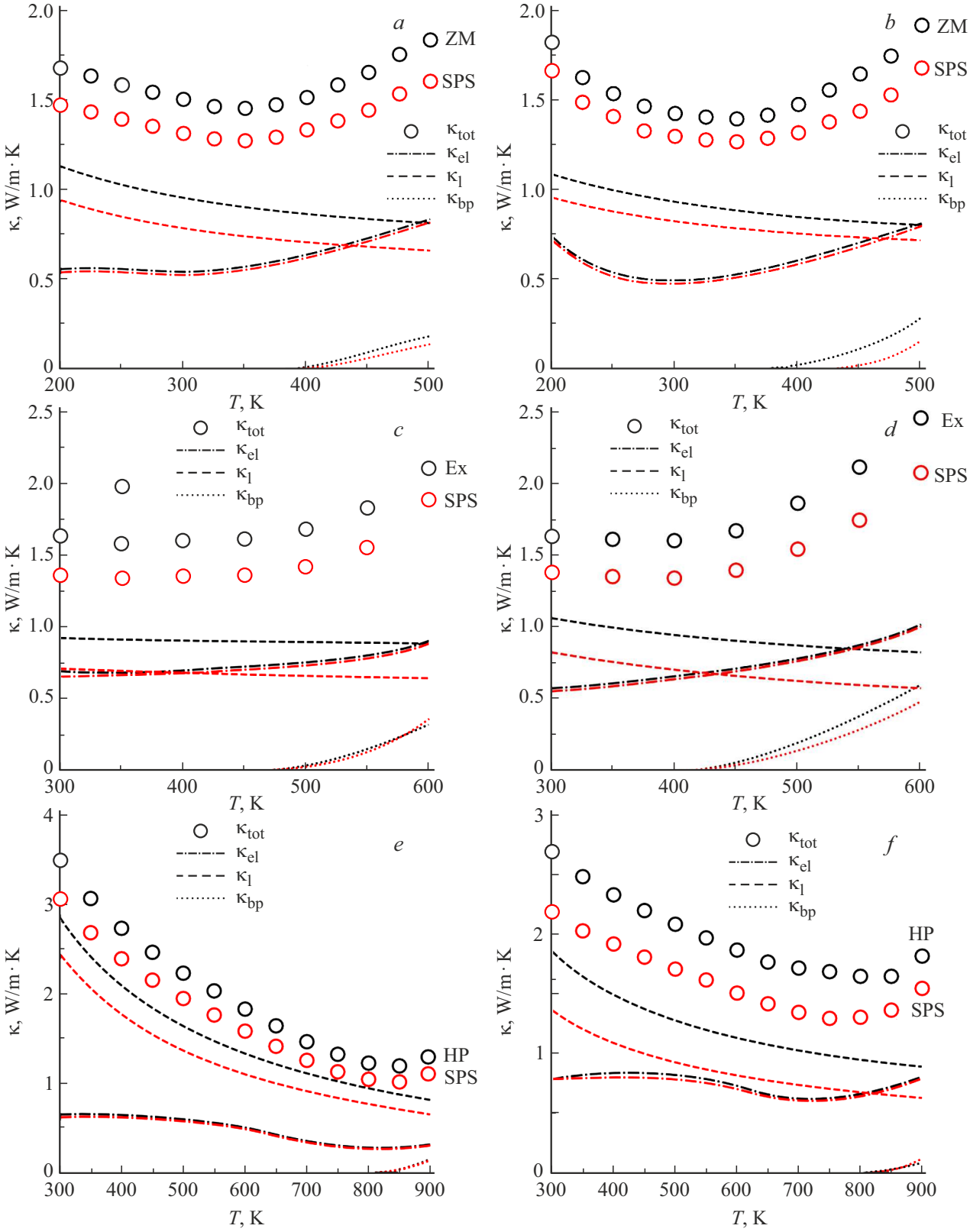

Figure 5. Experimental data on thermal conductivity and calculation results of its components for (*a*) $Bi_2Te_{2.8}Se_{0.2}$, (*b*) $Bi_{0.5}Sb_{1.5}Te_3$, (*c*) $Bi_2Te_{2.4}Se_{0.6}$, (*d*) $Bi_{0.4}Sb_{1.6}Te_3$, (*e*) PbTe, (*f*) GeTe.

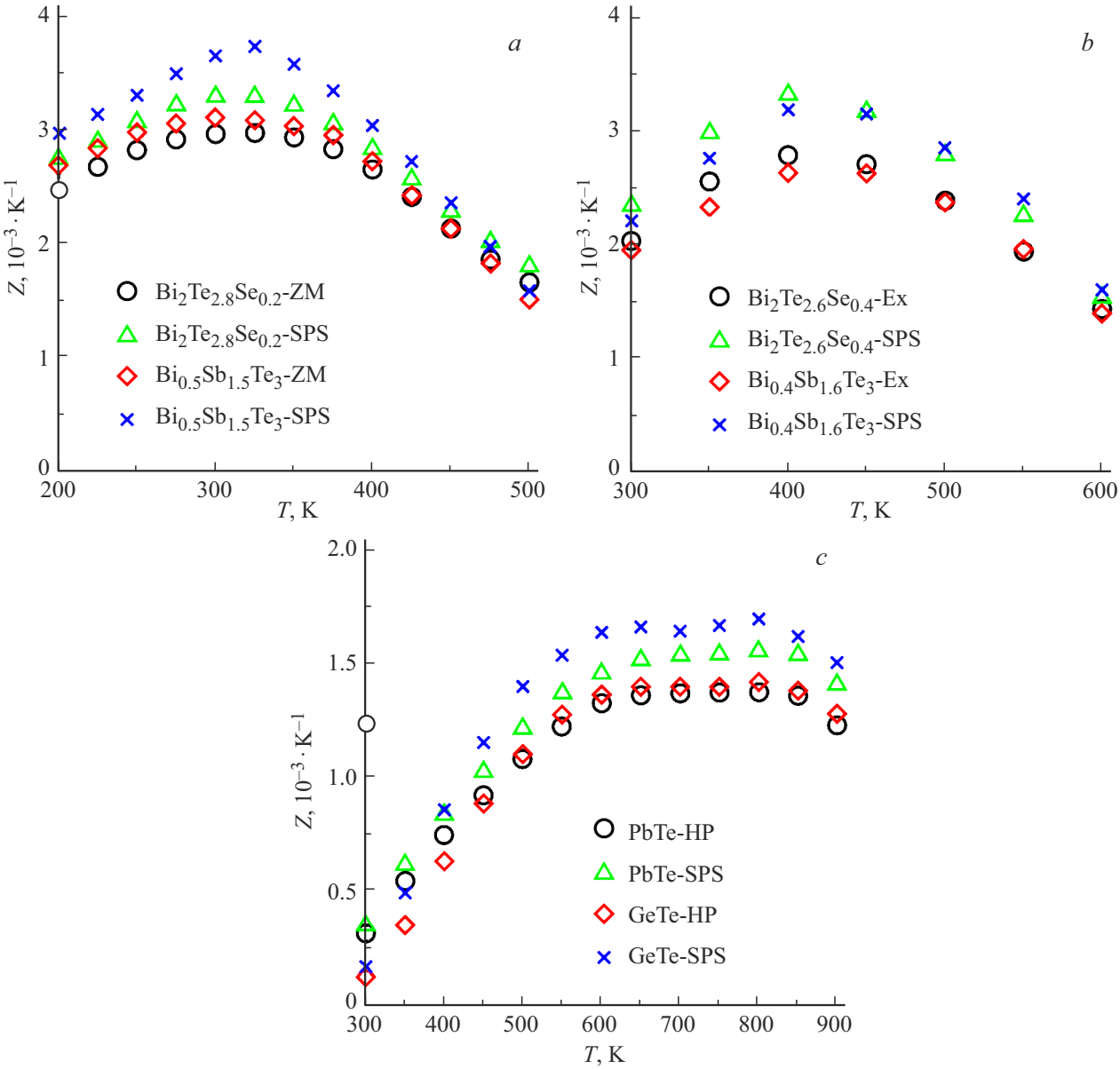

Figure 6. Temperature dependences Z: (*a*) $Bi_2Te_{2.8}Se_{0.2}$ and $Bi_{0.5}Sb_{1.5}Te_3$, (*b*) $Bi_2Te_{2.4}Se_{0.6}$ and $Bi_{0.4}Sb_{1.6}Te_3$, (*c*) PbTe and GeTe.

the main components of thermal conductivity to thermoelectric materials was established. In operating temperature ranges of thermoelectric materials, heat transport mechanisms are mainly determined by the phonon (κ_l), electron (κ_{el}) and bipolar (κ_{bp}) components of thermal conductivity [20,30–32]:

$$\kappa_{tot} = \kappa_l + \kappa_{el} + \kappa_{bp}. \quad (5)$$

The study of heat transport mechanisms was carried out for compositions of thermoelectric materials obtained by traditional methods and nanocrystalline materials. The components of thermal conductivity were calculated according to the method described in [33]. The results obtained are presented in Figure 5. Analyzing the mechanisms of heat transport, it can be argued that the observed decrease in thermal conductivity with an increase in temperature to minimum values at 330–340 K for $Bi_2Te_{2.8}Se_{0.2}$ and $Bi_{0.5}Sb_{1.5}Te_3$ (Figure 5, *a, b*) are determined by a drop of κ_l with a slight change in κ_{el} and in the absence of bipolar heat transport. After that, there is an increase in thermal conductivity due to κ_{el} and κ_{bp}, manifested in the region of 390–400 K. The electronic component makes a significant contribution to heat transport over the entire temperature range (about 30 %). The growth of κ_{tot} with the rise of temperature due to κ_{el} and κ_{bp} is determined by an increase in the contribution of minority charge carriers, which is confirmed by the results of temperature dependences of Seebeck coefficient and electrical conductivity. The results of the study of the temperature dependence of thermal conductivity for the considered thermoelectric materials are consistent with the data from [34–37]. Data obtained

Table 4. Maximal values Z of nanocrystalline and classic thermoelectric materials

Material	Nanocrystalline material		Classic material	
	Z_{max}, K^{-1}	T, K	Z_{max}, K^{-1}	T, K
$Bi_2Te_{2.8}Se_{0.2}$	$3.31 \cdot 10^{-3}$	330	$2.97 \cdot 10^{-3}$	320
$Bi_{0.5}Sb_{1.5}Te_3$	$3.72 \cdot 10^{-3}$	330	$3.10 \cdot 10^{-3}$	330
$Bi_2Te_{2.4}Se_{0.6}$	$3.30 \cdot 10^{-3}$	430	$2.79 \cdot 10^{-3}$	420
$Bi_{0.4}Sb_{1.6}Te_3$	$3.21 \cdot 10^{-3}$	440	$2.66 \cdot 10^{-3}$	420
PbTe	$1.59 \cdot 10^{-3}$	830	$1.37 \cdot 10^{-3}$	810
GeTe	$1.69 \cdot 10^{-3}$	820	$1.41 \cdot 10^{-3}$	820

by the authors of papers [38,39] covering bipolar thermal conductivity is slightly higher than our values. The values κ_{el} given in the work [40] correlate with the data we obtained.

Temperature dependences of thermal conductivity in the range 300–600 K and calculation data of its components for medium-temperature materials $Bi_2Te_{2.4}Se_{0.6}$ and $Bi_{0.4}Sb_{1.6}Te_3$ are shown in Figure 5, *c, d*. The thermal conductivity of these thermoelectric materials does not decrease significantly with the rise of temperature to 400 K. This is due to the fact that the decline in the phonon component is compensated by an increase in κ_{el}, which in these materials is about 30 %. With a further increase in temperature, the growth of κ_{tot} is determined by electronic heat transport and after 450 K — by bipolar heat transport. After 480 K, there is a significant increase in κ_{tot}, which is associated with an increase in the electronic and, to a greater extent, bipolar components of thermal conductivity. The onset of intrinsic conductivity leads to a decrease in thermoelectric figure of merit and determines the maximum operating temperatures of the thermoelectric material. The experimental values of the total thermal conductivity for thermoelectric materials produced by extrusion in [35,41–43], correlate with our data.

Experimental data on thermal conductivity and calculation results of its components for PbTe and GeTe based thermoelectric materials are shown in Figure 5, *e, f*. The decrease in thermal conductivity with the rise of temperature in these materials with a minimum in the range of 820 K is also due to a decrease in the phonon component, which declines by more than three times to this temperature. The electronic component, the contribution of which to heat transport is about 25 % for PbTe and 40% for GeTe, also decreases to the indicated temperatures. Then κ_{tot} stabilizes and there is a tendency to growth, which is associated with the appearance of bipolar heat transport, determined by an increase in the contribution of minority charge carriers. This result is confirmed by a change in the temperature dependences of electrical conductivity and Seebeck coefficient for these materials. Our experimental results correlate with the thermal conductivity data for PbTe [37,44–46] and GeTe [16,47–50].

Thus, it was found that for all the studied thermoelectric materials obtained by various methods, the nature of the change in the temperature dependences of the components of thermal conductivity is similar. The values of the electronic thermal conductivity for nanocrystalline and classical materials practically do not differ over the entire temperature range, and the bipolar components have similar values. The temperature changes of these components are consistent with the temperature dependences of electrical conductivity and Seebeck coefficient. The phonon thermal conductivity values of nanocrystalline materials are lower than those of classical ones and determine a corresponding decrease in total thermal conductivity, which is confirmed by the experimental data presented above. Thus, the results of the study of heat transport mechanisms confirm the fact of a decrease in the absolute value of thermal conductivity in nanocrystalline materials compared with classical materials due to the phonon component.

Based on the results of studies of thermoelectric parameters, the calculation of the thermoelectric figure of merit Z was carried out. Figure 6 shows the values of the temperature dependences of this parameter for classical and nanocrystalline materials. Table 4 shows the maximum values of the parameter Z for nanocrystalline and classical materials and the corresponding temperature values.

The thermoelectric figure of merit of nanocrystalline low-temperature materials based on $Bi_2Te_{2.8}Se_{0.2}$ increases by

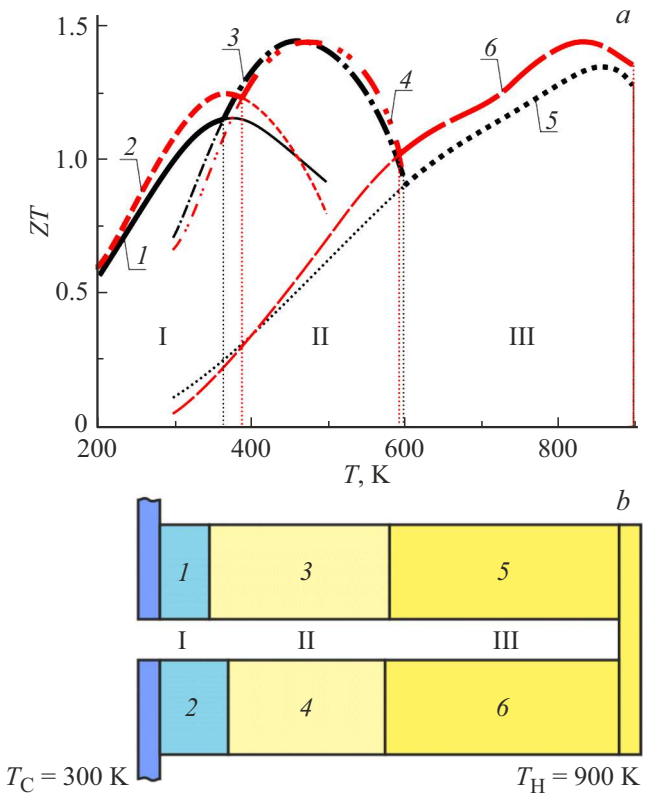

Figure 7. (*a*) Temperature dependences ZT of thermoelectric materials *1*) $Bi_2Te_{2.8}Se_{0.2}$; *2*) $Bi_{0.5}Sb_{1.5}Te_3$; *3*) $Bi_2Te_{2.4}Se_{0.6}$; *4*) $Bi_{0.4}Sb_{1.6}Te_3$; *5*) PbTe; *6*) GeTe; (*b*) — Structure of three-sectional (I–III sections) thermoelement.

no more than 11 %, and based on $Bi_{0.5}Sb_{1.5}Te_3$ by 20,% compared to the classic materials. Such a difference for materials *n*- and *p*-types of conductivity is determined by the size of crystallites in these nanocrystalline materials and, accordingly, the efficiency of phonon scattering, which affects the values of thermal conductivity. The nanocrystalline $Bi_2Te_{2.8}Se_{0.2}$ have average crystallite size of about 97 nm, and $Bi_{0.5}Sb_{1.5}Te_3$ — 76 nm. For the nanocrystalline materials based on $Bi_2Te_{2.4}Se_{0.6}$ and $Bi_{0.4}Sb_{1.6}Te_3$ the increase in Z reaches 18−21 %, compared with classic materials. PbTe-based nanocrystalline material have values of Z higher than the thermoelectric figure of merit of the classical material obtained by hot pressing by no more than 14 %. This is due to the fact that PbTe is the most problematic material in terms of obtaining nanocrystalline samples. It was not possible to obtain average crystallite sizes of less than 100 nm for nanocrystalline PbTe, which does not significantly reduce the phonon component of thermal conductivity. For nanocrystalline GeTe, the obtained values of Z by 21 % exceed the values of Z samples obtained by hot pressing. A certain discrepancy between a decrease in thermal conductivity and an increase in Z in nanocrystalline materials is explained by lower value of electrical conductivity in the latter.

Thus, the studied thermoelectric materials have high values of Z for practically used classical thermoelectric materials. The values of Z for nanocrystalline materials correspond to the maximum reproducible values obtained by other authors [11,16,51–57].

As a result of the study, the temperature dependences of the dimensionless thermoelectric figure of merit (ZT) for nanocrystalline thermoelectric materials are presented (Figure 7, *a*). Using the results obtained according to the methodology presented in [58], a three-section thermoelement was calculated (Figure 7, *b*). The efficiency of 18 % was obtained. The simulation results do not take into account the thermal and electrical losses at the electrical contacts.

4. Conclusion

Traditional methods and nano-structuring were used to fabricate and study the thermoelectric materials on the basis of $Bi_2Te_{3-x}Se_x$, $Bi_{2-x}Sb_xTe_3$, PbTe and GeTe, designed to manufacture thermoelements capable of operating within the temperature range 200−900 K. As a result of the study of the basic physical properties, their closeness has been established for nanocrystalline and materials obtained by traditional methods of the same composition. Studies of the thermoelectric parameters for each material have been carried out and their high thermoelectric figure of merit has been established. The mechanisms of heat transport in the operating temperature range are determined and the components of thermal conductivity of thermoelectric materials are found. It has been established that the decrease in total thermal conductivity is determined by the phonon component, which is lower in nanocrystalline materials. Because of this, Z of the nanocrystalline materials is higher by 10−21 %. The relationship between the structure and thermoelectric parameters has been established for nanocrystalline materials. The obtained results confirm feasibility of fabrication of nanocrystalline materials in order to reduce phonon thermal conductivity and increase Z.

As a result of modeling a three-sectional thermoelement with operating temperatures 300−900 K, in the structure of which nanocrystalline thermoelectric materials are used, a high efficiency value of 18 % was obtained.

Funding

This study was supported by the Russian Science Foundation (project No. 20-19-00494).

Conflict of interest

The authors declare that they have no conflict of interest.

References

[1] X.-L. Shi, J. Zou, Z.-G. Chen. Chem. Rev. **120**, *15*, 7399 (2020).
[2] P. Ren, Y. Liu, J. He, T. Lv, J. Gao, G. Xu. Inorg. Chem. Front. **5**, *10*, 2380 (2018).
[3] A.A. Sherchenkov, Yu.I. Shtern, R.E. Mironov, M.Yu. Shtern, M.S. Rogachev. Nanotechnol. Russia **10**, *11–12*, 827 (2015).
[4] S. Ghosh, L. Raman, S. Sridar, W. Li. Crystals **14**, *5*, 432 (2024).
[5] P. Baskaran, M. Rajasekar. RSC Adv. **14**, *30*, 21706 (2024).
[6] A.A. Sherchenkov, Yu.I. Shtern, M.Yu. Shtern, M.S. Rogachev. Nanotechnol. Russia **11**, *7–8*, 387 (2016).
[7] C. Zhao, Z. Li, T. Fan, C. Xiao, Y. Xie. Research **2020**, 9652749 (2020).
[8] Z. Wu, S. Zhang, Z. Liu, E. Mu, Z. Hu. Nano Energy **91**, 106692 (2022).
[9] R. Freer, A.V. Powell. J. Mater. Chem. C **8**, *2*, 441 (2020).
[10] M. Maksymuk, B. Dzundza, O. Matkivsky, I. Horichok, R. Shneck, Z. Dashevsky. J. Power Sources **530**, 231301 (2022).
[11] T. Parashchuk, A. Shabaldin, O. Cherniushok, P. Konstantinov, I. Horichok, A. Burkov, Z. Dashevsky. Physica B: Condens. Matter. **596**, 412397 (2020).
[12] Y. Saberi, S.A. Sajjadi. J. Alloys Compd. **904**, 163918 (2022).
[13] J. Mao, Z. Liu, J. Zhou, H. Zhu, Q. Zhang, G. Chen, Z. Ren. Adv. Phys. **67**, *2*, 69 (2018).
[14] A. Bharwdaj, K.S. Jat, S. Patnaik, Yu.N. Parkhomenko, Y. Nishino, V.V. Khovaylo. Nanotechnol. Russia **14**, *7–8*, 281 (2019).
[15] B. Cai, H. Hu, H.-L. Zhuang, J.-F. Li. J. Alloys Compd. **806**, 471 (2019).
[16] Z. Dashevsky, I. Horichok, M. Maksymuk, A.R. Muchtar, B. Srinivasan, T. Mori. J. Am. Ceram. Soc. **105**, *6*, 4500 (2022).
[17] Y. Shtern, A. Sherchenkov, M. Shtern, M. Rogachev, D. Pepelyaev. Mater. Today Commun. **37**, 107083 (2023).
[18] L.-D. Zhao, V.P. Dravid, M.G. Kanatzidis. Energy Environ. Sci. **7**, *1*, 251 (2014).

[19] G. Tan, L.-D. Zhao, M.G. Kanatzidis. Chem. Rev. **116**, *19*, 12123 (2016).
[20] D.K. Aswal, R. Basu, A. Singh. Energy Conv. Manag. **114**, 50 (2016).
[21] L.P. Bulat, I.A. Drabkin, V.V. Karataev, V.B. Osvenskiĭ, D.A. Pshenaĭ-Severin. Phys. Solid State **52**, *9*, 1836 (2010).
[22] L.P. Bulat, D.A. Pshenay-Severin, V.B. Osvenskii, Yu.N. Parkhomenko. Semiconductors **51**, *6*, 695 (2017).
[23] A. Sherchenkov, N. Borgardt, M. Shtern, Y. Zaytseva, Y. Shtern, M. Rogachev, V. Sazonov, A. Yakubov, D. Pepelyaev. Mater. Today Energy **37**, 101416 (2023).
[24] M.Yu. Shtern. Semiconductors **56**, *13*, 437 (2022).
[25] M.Yu. Shtern. In: 2019 IEEE Conference of Russian Young Researchers in Electrical and Electronic Engineering (EIConRus) / Ed. S. Shaposhnikov. IEEE, St. Petersburg, Moscow. (2019).
[26] M.Yu. Shtern, L.I. Matyna, M.S. Rogachev, A.P. Merlyan. In: 2021 IEEE Conference of Russian Young Researchers in Electrical and Electronic Engineering (ElConRus) / Ed. S. Shaposhnikov. IEEE, St. Petersburg, Moscow. (2021).
[27] M. Shtern, A. Sherchenkov, Y. Shtern, N. Borgardt, M. Rogachev, A. Yakubov, A. Babich, D. Pepelyaev, I. Voloshchuk, Y. Zaytseva, S. Pereverzeva, A. Gerasimenko, D. Potapov, D. Murashko. J. Alloys Compd. **946**, 169364 (2023).
[28] T. Hayashi, M. Sekine, J. Suzuki, Y. Horio, H. Takizawa. Mater. Trans. **48**, *10*, 2724 (2007).
[29] M.Yu. Shtern, M.S. Rogachev, A.A. Sherchenkov, Yu.I. Shtern. Mater. Today: Proceedings **20**, 295 (2020).
[30] G.S. Nolas, J. Sharp, H.J. Goldsmid. Thermoelectrics: Basic Principles and New Materials Developments. Springer Berlin Heidelberg, Berlin. (2001). 293 p.
[31] L.D. Zhao, H.J. Wu, S.Q. Hao, C.I. Wu, X.Y. Zhou, K. Biswas, J.Q. He, T.P. Hogan, C. Uher, C. Wolverton, V.P. Dravid, M.G. Kanatzidis. Energy Environ. Sci. **6**, *11*, 3346 (2013).
[32] D.M. Rowe, C.M. Bhandari. Modern thermoelectric. Reston Publishing Company, London. (1983). 157 p.
[33] M.S. Rogachev, M.Yu. Shtern, Yu.I. Shtern. Nanotechnol. Russia **16**, *3*, 308 (2021)
[34] L.D. Ivanova, L.I. Petrova, Yu.V. Granatkina, V.S. Zemskov, O.B. Sokolov, S.Ya. Skipidarov, N.I. Duvankov. Inorg. Mater **45**, *2*, 123 (2009).
[35] L.D. Ivanova, L.I. Petrova, Yu.V. Granatkina, V.S. Zemskov, O.B. Sokolov, S.Ya. Skipidarov, V.A. Kurganov, V.V. Podbel'skii. Inorg. Mater **47**, *5*, 459 (2011).
[36] M.A. Korzhuev, L.D. Ivanova. Inorg. Mater **42**, *7*, 712 (2006).
[37] K.T. Wojciechowski, T. Parashchuk, B. Wiendlocha, O. Cherniushok, Z. Dashevsky. J. Mater. Chem. C **8**, *38*, 13270 (2020).
[38] Y. Zheng, Q. Zhang, X. Su, H. Xie, S. Shu, T. Chen, G. Tan, Y. Yan, X. Tang, C. Uher, G.J. Snyder. Adv. Energy Mater. —bf5, *5*, 1401391 (2015).
[39] Y. Zheng, G. Tan, Y. Luo, X. Su, Y. Yan, X. Tang. Mater. **10**, *6*, 617 (2017).
[40] Y. Zheng, H. Xie, S. Shu, Y. Yan, H. Li, X. Tang. J. Electron. Mater. **43**, *6*, 2017 (2014).
[41] L.-P. Hu, T.-J. Zhu, Y.-G. Wang, H.-H. Xie, Z.-J. Xu, X.-B. Zhao. NPG Asia Mater. **6**, *2*, e88 (2014).
[42] X. Wang, J. Yu, R. Zhao, B. Zhu, N. Gao, B. Xiang, Y. Yu, K. Zhang, Z. Huang, F. Zu. J. Phys. Chem. Sol. **124**, 281 (2019).
[43] L.D. Ivanova, L.I. Petrova, Yu.V. Granatkina, V.S. Zemskov, O.B. Sokolov, S.Ya. Skipidarov, N.I. Duvankov. Inorg. Mater **44**, *7*, 687 (2008).
[44] M.H. Lee, J.H. Park, S.-D. Park, J.-S. Rhyee, M.-W. Oh. J. Alloys Compd. **786**, 515 (2019).
[45] D. Wang, Y. Qin, S. Wang, Y. Qiu, D. Ren, Y. Xiao, L. Zhao. Annalen der Physik **532**, *11*, 1900421 (2020).
[46] S.N. Girard, J. He, X. Zhou, D. Shoemaker, C.M. Jaworski, C. Uher, V.P. Dravid, J.P. Heremans, M.G. Kanatzidis. J. Am. Chem. Soc. **133**, *41*, 16588 (2011).
[47] Y. Gelbstein, J. Davidow, S.N. Girard, D.Y. Chung, M. Kanatzidis. Adv. Energy Mater. **3**, *6*, 815 (2013).
[48] Y. Qiu, Y. Jin, D. Wang, M. Guan, W. He, S. Peng, R. Liu, X. Gao, L.-D. Zhao. J. Mater. Chem. A **7**, *46*, 26393 (2019).
[49] Y. Jin, Y. Xiao, D. Wang, Z. Huang, Y. Qiu, L.-D. Zhao. ACS Appl. Energy Mater. **2**, *10*, 7594 (2019).
[50] S. Perumal, M. Samanta, T. Ghosh, U.S. Shenoy, A.K. Bohra, S. Bhattacharya, A. Singh, U.V. Waghmare, K. Biswas. Joule **3**, *10*, 2565 (2019).
[51] C. Lee, P. Dharmaiah, D.H. Kim, D.K. Yoon, T.H. Kim, S.H. Song, S.-J. Hong. ACS Appl. Mater. Interfaces **14**, *8*, 10394 (2022).
[52] L. Xie, H. Qin, J. Zhu, L. Yin, D. Qin, F. Guo, W. Cai, Q. Zhang, J. Sui. Adv. Electron. Mater. **6**, *2*, 1901178 (2020).
[53] Z. Wang, G. Wang, R. Wang, X. Zhou, Z. Chen, C. Yin, M. Tang, Q. Hu, J. Tang, R. Ang. ACS Appl. Mater. Interfaces **10**, *26*, 22401 (2018).
[54] D.-Z. Wang, W.-D. Liu, X.-L. Shi, H. Gao, H. Wu, L.-C. Yin, Y. Zhang, Y. Wang, X. Wu, Q. Liu, Z.-G. Chen. J. Mater. Sci. Technol. **106**, 249 (2022).
[55] H.-S. Yen, J.-F. Lin, S.-C. Shi, H.-T. Lin, J.-C. Chiu. Mater. Res. Express **11**, *2*, 026304 (2024).
[56] H. Mansouri, S.A. Sajjadi, A. Babakhani, Y. Saberi. J. Mater. Sci.: Mater. Electron. **32**, *8*, 9858 (2021).
[57] W. Liu, T. Hong, S. Dong, D. Wang, X. Gao, Y. Xiao, L.-D. Zhao. Mater. Today Energy **26**, 100983 (2022).
[58] M.Yu. Shtern, M.S. Rogachev, Y.I. Shtern, A.A. Sherchenkov, A.O. Kozlov. In: 2019 International Seminar on Electron Devices Design and Production (SED). IEEE, Prague, Czech Republic. (2019).

Translated by T.Zorina